Multiple nerve rings coordinate *Hydra* mechanosensory behavior

Krishna N. Badhiwala[1], Abby S. Primack[2], Celina E. Juliano[2], Jacob T. Robinson*[1,3,4]

1. Department of Bioengineering, Rice University, 6100 Main Street, Houston, Texas 77005
2. Department of Molecular and Cellular Biology, University of California, Davis, CA, USA.
3. Department of Electrical and Computer Engineering, Rice University, 6100 Main Street, Houston, Texas 77005
4. Department of Neuroscience, Baylor College of Medicine, One Baylor Plaza, Houston, Texas, 77030

*Correspondence to: jtrobinson@rice.edu.

Abstract

Hydra vulgaris is an emerging model organism for neuroscience due to its small size, transparency, genetic tractability, and regenerative nervous system; however, fundamental properties of its sensorimotor behaviors remain unknown. Here, we use microfluidic devices combined with fluorescent calcium imaging and surgical resectioning to study how the nervous system coordinates *Hydra*'s mechanosensory response. We find that mechanical stimuli cause animals to contract, and this response relies on both the oral and aboral nerve rings. We also find that these nerve rings work together to coordinate spontaneous contractions suggesting that spontaneous behavior and sensorimotor responses converge on to a common neural circuit. These findings improve our understanding of how *Hydra*'s diffuse nervous system supports sensorimotor behaviors, which is needed to increase the utility of *Hydra* as a model organism for neuroscience.

Introduction

By studying the nervous systems of diverse model organisms, it may be possible to discover fundamental principles relating neural activity and behaviors. Animals have evolved different neural structures like the nerve net (e.g. *Hydra*), nerve cords and ganglia (e.g. *C. elegans*, *Aplysia*, planaria) and brain (e.g. *Drosophila*, zebrafish, rodents, and primates). Despite the vastly different structures, many behaviors are conserved across species, including sensorimotor responses[1–6] and sleep[7–15]. By comparing neural circuits that support similar

behaviors despite different architectures, we can discover organizational principles of neural circuits that reflect millions of years of evolutionary pressure. While there are many potential organisms that would support this type of comparative neuroscience, only a small group of animals have the qualities to support laboratory experiments: short generation span, ease of breeding and manipulation in laboratory conditions, small and compact size, optical transparency, and well-developed genetic toolkit.

Transparent, millimeter-sized animals in particular offer a number of advantages for neuroscientists because it is possible to image neural activity throughout the entire nervous system using genetically-encoded calcium or voltage-sensitive fluorescent proteins[16–25]. In addition, some millimeter-sized animals are compatible with microfluidic devices for precise environmental control and microscopy techniques that offer cellular-resolution functional imaging of the entire nervous system. These properties, combined with genetic tractability, provide a powerful way of revealing neuronal dynamics across the entire nervous system (not just a small region) during behaviors. For instance, whole nervous system imaging of confined or freely moving animals has revealed the neuronal dynamics underlying locomotion[19,26] and sensory motivated global state transitions in *C. elegans*[27,28], responses to noxious odor and visuomotor behaviors in zebrafish[19–24], responses to light and odor in *Drosophila*[18,29], and neuronal ensembles correlated with basal behaviors and response to light in *Hydra*[30,31].

Hydra is unique among the small, transparent organisms discussed above due to its regenerative ability and highly dynamic nervous system. While most small, transparent model systems (like *C. elegans* or zebrafish larvae) suffer permanent behavioral deficits from the loss of one or a few neurons[32–36], *Hydra* can completely recover from a significant neuronal loss to regain normal contractile behavior in as little as ~ 48 hours[37–39]. This radially symmetric freshwater cnidarian has a nervous system composed of two diffuse networks of neurons, one embedded in the endoderm and another embedded in the ectoderm[40,41]. While this diffuse nerve net in *Hydra* is highly dynamic with continuous cellular turnover and migration[42,43], there are regions with slower neuronal turnover compared to the rest of the nerve net where increased neuronal density resembling nerve rings are found[44–46] (Fig. 1a). One of these regions is in the oral end in the apex above the ring of tentacles (“hypostomal nerve ring”), another in the aboral end in the foot (“peduncle nerve ring”) (Fig. 1a). Recent single-cell RNA sequencing has provided a complete molecular and spatial map of the *Hydra* nervous system, including identification of unique cell-type specific biomarkers to generate new transgenic models[47]. This existing molecular and spatial map of the nervous system suggests there is no overlap in the neuronal cell types that make up the hypostomal and peduncle nerve rings and the distribution of the cell types varies along the length of the body (Fig. 1b). Finally, the demonstration of

microfluidic and transgenic tools combined with *Hydra's* dynamic yet 'simple' neural architecture has enabled observations of basal and sensory motivated behaviors in the regenerating nervous system[31].

To better establish *Hydra* as a model organism for comparative neuroscience, it is critical to understand their basic sensorimotor behaviors, such as response to touch. While it has been well documented that *Hydra* contract when mechanically agitated or poked with a pipette[48–53], we found no quantitative reports of how this behavior depends on stimulus intensity or is mediated by neural activity. Although significant insights in *Hydra* behavior have been possible over the last several decades with simple methodologies and manual observations, including that the tentacles and/or the hypostome are needed for mechanosensory response, these experiments lack quantitative characterization of neuronal or behavioral response. Forceps-induced touch allowed local stimulation but it is difficult to control the force applied manually[54,55]. The force applied by pinching the body could have been strong enough to induce a response in the nerve-free animals similar to that observed from non-neuronal cell cultures. While stimulation with mechanical agitation allowed control over stimulus intensity, these observations were limited to changes in body lengths[52].

Here, we use whole animal functional imaging combined with resection studies to discover that despite the apparently diffuse nerve net in *Hydra*, these animals process sensorimotor responses primarily in regional networks. To study the mechanosensory response, we first developed a microfluidic system to apply a local mechanical stimulus and quantify *Hydra's* behavioral and neural response. We then measured these responses in the absence of select regions of the body and found at least one of the nerve rings, hypostome (oral) or the peduncle (aboral), is required to coordinate spontaneous contractions, though the oral network plays a more significant role. We found a significant reduction in the mechanosensory response with the removal of the hypostome, the region where sensory information is likely processed. These sensorimotor experiments combined with whole-animal neural and epitheliomuscular imaging reveal that *Hydra* is capable of receiving sensory information along the body column, however, the oral region is necessary for coordinating the motor response.

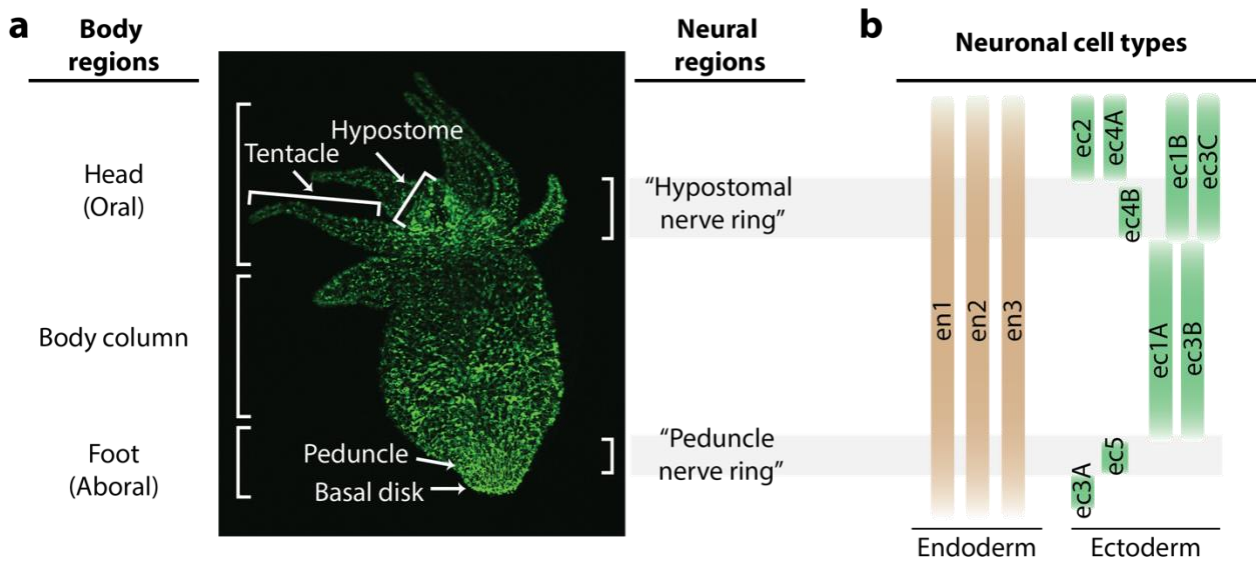

Figure 1: Distribution of neurons in the *Hydra* nerve net. a) Fluorescence image of *Hydra* nerve net. Green fluorescent protein (GFP) is expressed in neurons (nGreen transgenic line[47]). Body anatomy annotated on the left. White arrows indicate the body parts: hypostome, tentacles, peduncle and basal disk. High neuronal density regions on the right. b) Distribution of neuronal cell types varying longitudinally along the body. Cell types identified through single cell RNA sequencing[47]. Endodermal nerve net cell types in orange. Ectodermal nerve net cell types in green.

Results

Hydra's mechanosensory response is dependent on stimulus intensity

To better understand sensory information processing in *Hydra*, we developed a double-layer microfluidic system that can apply a local mechanical stimulus while we image the response of the entire nervous system using fluorescence microscopy (Fig. 2, Supp. Movie 1). This local mechanical stimulation is made possible by push-down microfluidic valves (Fig. 2a) that deliver mechanical stimuli to a portion of the *Hydra* body with precise temporal and spatial control (see "Methods"). For all experiments, we pressurized a valve (400 µm diameter) that was directly above the animal (for 1 sec every 31 sec, see "Methods") to poke the body column while simultaneously performing functional calcium imaging (Fig. 2b).

Using our microfluidic platform, we sought to characterize *Hydra's* sensitivity to local touch and the associated neural response. We performed experiments using transgenic *Hydra* expressing GCaMP6s in neurons[56]. When we delivered mechanical stimuli, we found bright calcium signals generated by a small number of neurons in the hypostome and body column, and a striking co-activation of many neurons in the ectodermal peduncle nerve ring (Fig. 2b). This nerve ring activity appeared as either a single bright calcium spike (or "contraction pulse") or a volley of

bright calcium spikes (or “contraction burst”). The calcium spikes appear to be similar to the pattern of neural activity correlated with spontaneous (or basal) body contractions that occur in absence of stimuli (Fig. 2c and Supp. Movie 2, 3)[56,57]. From here after, we define *Hydra’s* “mechanosensory response” as calcium spikes in the peduncle nerve ring and the associated behavioral contractions if they occur within one second of a mechanical stimulus (Fig. 2c, d and Supp. Fig.1).

Using fluorescence calcium imaging of neurons in the peduncle region during mechanical stimulation, we found that the probability of the mechanosensory response depends on the intensity of the stimulus, which is consistent with many psychometric functions (Fig. 2e). *Hydra* were more than five times more likely to contract within one second of receiving a strong mechanical stimulus than during a random one second interval without a stimulus (Stimulus valve pressure 20 and 25 psi; probability of response = 0.60 ± 0.06 and 0.77 ± 0.08, mean ± SEM, respectively; No stimulus valve pressure = 0 psi; probability of response = 0.11 ± 0.01, mean ± SEM; Fig. 2e,h). During mild stimuli, there was a slight increase (~ 2x) in response probability above the spontaneous activity, although this increase was not statistically significant compared to spontaneous contractions (valve pressure 10 and 15 psi; probability of response = 0.23 ± 0.01 and 0.24 ± 0.03, mean ± SEM, respectively; Fig. 2e,h). We found that *Hydra* did not respond to a weak mechanical stimulus that corresponded to a valve pressure of 5 psi (probability of response = 0.09 ± 0.02, mean ± SEM; Fig. 2e,h).

Further analysis of the contractile activity pattern revealed that the contractions were more frequent and shorter in duration when we repeated mechanical stimulation every 31 seconds for one hour. While spontaneous body contractions are observed roughly once every minute in microfluidics, when we stimulated *Hydra* with a strong mechanical stimuli we found that the frequency nearly matches the 31 sec between stimuli (Interval between spontaneous contractions = 72.98 sec ± 4.58, mean ± SEM; 66.68 ± 5.73 sec median ± SE; Interval between stimulated contractions = 20 psi, 38.28 ± 1.77 sec, mean ± SEM; 31.14 ± 2.21 sec, median ± SE; 25 psi, 32.20 ± 1.04 sec, mean ± SEM; 31.14 ± 1.30 sec, median ± SE; Fig. 2f,h). While the majority of spontaneous contractions contain a burst of two or more contraction pulses, stimulated contractions were roughly three times more likely to be a single pulse contraction (Percentage of spontaneous contractions that are a single pulse = 0psi, 16.87 ± 5.38 % mean ± SEM; Percentage of stimulated contractions that are a single pulse = 20 psi, 56.84 ± 2.48%; 25psi, 62.50 ± 5.23 %, mean ± SEM; Fig. 2g,h).

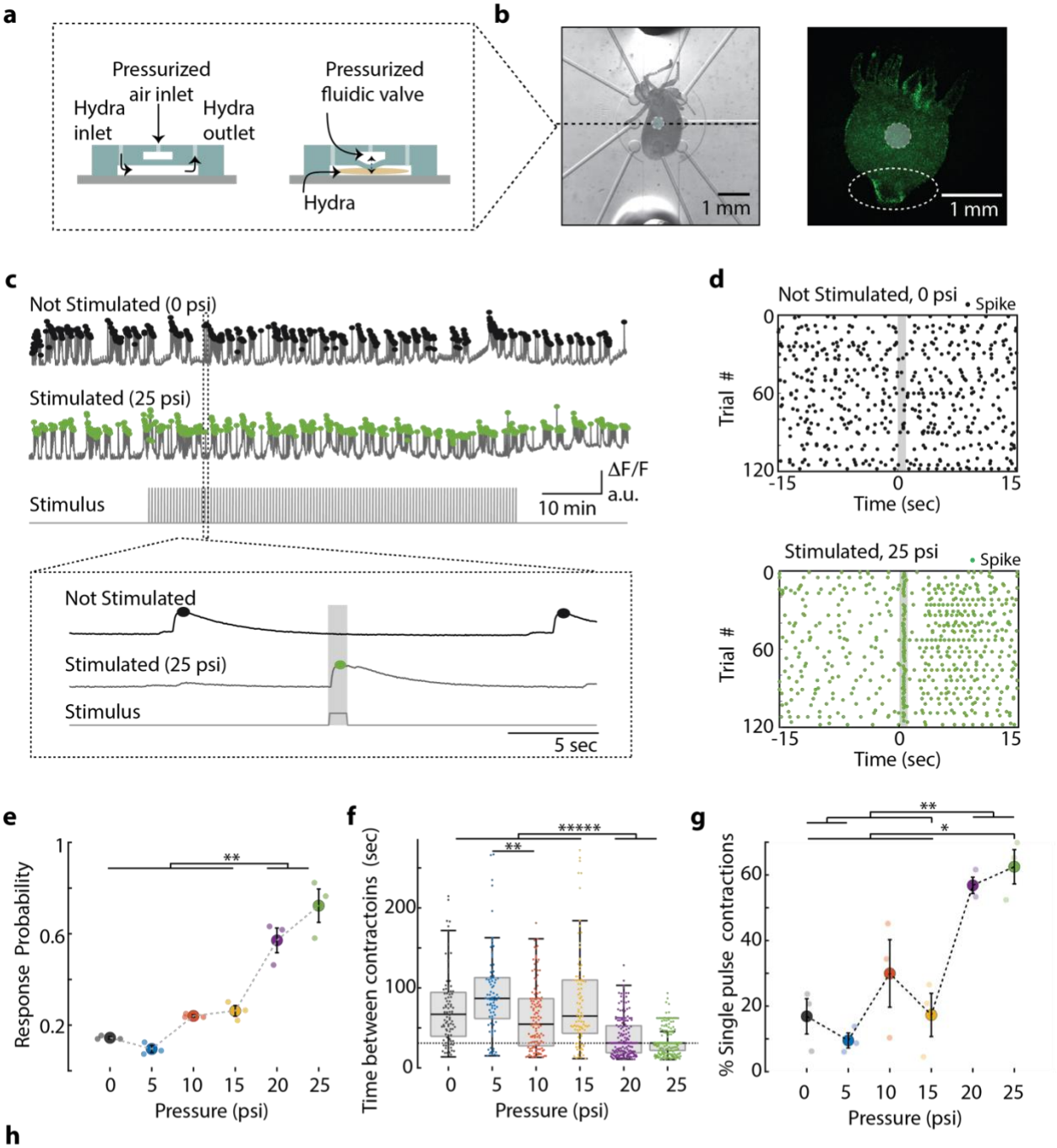

h

Pressure (psi)	Response probability mean +/- SEM	Time between contractions mean +/- SEM	Time between contractions median +/- SE	Single pulse contractions mean +/- SEM
0	0.11 +/- 0.01	72.98 +/- 4.58 sec	66.68 +/- 5.73 sec	16.87 +/- 5.38 %
5	0.09 +/- 0.02	92.66 +/- 5.87 sec	86.65 +/- 7.35 sec	9.52 +/- 2.27 %
10	0.23 +/- 0.01	63.01 +/- 3.73 sec	54.73 +/- 4.67 sec	29.96 +/- 10.29 %
15	0.24 +/- 0.03	83.60 +/- 6.37 sec	64.73 +/- 7.98 sec	17.30 +/- 6.59 %
20	0.60 +/- 0.06	38.28 +/- 1.77 sec	31.14 +/- 2.21 sec	56.84 +/- 2.48 %
25	0.77 +/- 0.08	32.20 +/- 1.04 sec	31.14 +/- 1.30 sec	62.50 +/- 5.23 %

Figure 2: *Hydra's* mechanosensory response is dependent on stimulus intensity. a) Side view of double-layer microfluidic device for mechanical stimulation (left). Device with pressurized valve (right). *Hydra* is immobilized in the bottom *Hydra* layer. Compressed air input into the valve layer causes the circular membrane (400 um diameter) to push down on *Hydra* (right). b) Brightfield image (left) of *Hydra* immobilized in the bottom layer of the chip and the arrangement of micro-valves on the top layer. Micro-valve used for stimulation falsely colored with a light blue circle. Fluorescence image (right) of *Hydra* with pan-neuronal expression of GCaMP6s. White dashed circle marks the peduncle region of interest (ROI) used for quantifying calcium fluorescence changes. c-d) Representative calcium fluorescence activity in the peduncle region from an animal not stimulated and animal mechanically stimulated with 25 psi. Black and green dots indicate fluorescence (calcium) spikes. Gray shaded regions indicate stimulus 'on' time (also "response window"). c) Fluorescence (calcium) trace from *Hydra* not stimulated (top) and stimulated with 25 psi (middle). Stimulation protocol in gray (bottom trace): 20 min no stimulation, 1 hr of repeated stimulation (1 sec 'on', 30 sec 'off') and 20 min no stimulation. Stimulus 'on' times indicated with vertical lines. Zoom-in of 30 sec fluorescence and stimulation protocol trace from one stimulation trial. d) Raster plot of stimulus time aligned spiking activity from multiple trials superimposed for Hydra not stimulated (top) and stimulated with 25 psi (bottom). e). Mechanosensory response probability, fraction of trials (out of 119 total) that have at least one spiking event (also contraction pulse) occurring during the 1 sec response window (gray shaded region) when valve is pressurized. Large circles indicate average probability from all animals (N=3) combined for each condition. Small circles indicate probability from a single animal. (one-way anova with post hoc bonferroni correction, largest $p < 0.01$). f). Time interval between body contractions under each condition. Dashed line represents the time interval between stimuli (~31 sec). (Kruskal-wallis with post-hoc dunn-sidak correction). g). Percent of all body contractions that are a single pulse (one-way anova with post-hoc bonferroni correction). (Error bars are standard error of mean (SEM.); N = 3 *Hydra* for each condition; * = $p < 0.05$, ** = $p < 0.01$, ***** = $p < 0.00001$). h) Table summarizing the mechanosensory response probability, time between contractions and percent of contractions that are single pulses for each stimulus intensity (mean **±** SEM or median **±** SE).

Hydra's mechanosensory response is mediated by the nerve net

Based on the latency of the mechanosensory response, we hypothesized that sensorimotor information is transmitted by electrical activity in the *Hydra* nerve net and is not mediated by passive calcium diffusion through ectodermal cells. This hypothesis is supported by the fact that aneural *Hydra,* which no longer spontaneously contract in absence of stimuli, are capable of aversive contractile response to touch, however, their responses are slow and require strong mechanical stimulus[54,55]. To further test our hypothesis, we created a transgenic *Hydra* strain that expresses the calcium indicator GCaMP7b (under the EF1α promoter, see 'Methods') in the ectodermal epitheliomuscular cells. With this transgenic line we could measure contraction pulses and contraction bursts by averaging calcium activity in all the epitheliomuscular cells (Supp. Fig. 2). We hypothesized that if the mechanosensory response was primarily mediated by the epitheliomuscular cells, we would expect to see propagation of calcium activity from the site of the stimulation. However, this was not the case. Instead we observed fast propagation of calcium activity throughout the entire ectoderm. Imaging calcium activity in the peduncle neurons showed that changes in neural activity were correlated with the observed changes in epithelial muscle cells with increasing stimulus intensity (Fig. 2 and Supp. Fig. 3), suggesting that changes in behavior are indeed mediated by the nervous systems and not the result of epitheliomuscular activity alone. Although *Hydra*'s behavioral responses are slow compared to other invertebrates, the 0.5 sec average response time in our data could not be explained by

calcium diffusion alone, which would take ~ 100 sec to travel the average distance of ~ 0.5 - 1 mm between stimulation site and the peduncle or hypostome (Supp. Fig. 4a). Our data show the calcium signals from the peduncle neurons or ectodermal muscles started increasing within ~ 0.1 - 0.2 sec reaching peak fluorescence at ~ 0.5 - 0.6 sec regardless of the stimulus intensity (Supp. Fig. 4b,c). We found no difference in the calcium response times between neural and muscle calcium imaging, though this could be influenced by the dynamics of the calcium indicator, which typically cannot give information about latencies less than 50 ms[17].

Aboral region is not necessary for mechanosensory response in *Hydra*

Having quantitatively established *Hydra's* sensorimotor response to mechanical stimuli, we next asked if there are specific regions of the nervous system that play primary roles in mediating this response. Patch-clamp electrophysiology of individual neurons in *Hydra* has thus far been unsuccessful despite attempts by many research groups, and minimally invasive, and cell-type specific neuromodulation techniques such as optogenetics have yet to be developed for *Hydra*. However, the animal's regenerative abilities allow us to resect large portions of tissue without killing the animal, and thus we can borrow from the tradition of lesioning brain regions to study their functions[52,58–61].

Because the *Hydra* body plan is radially symmetric with cell types primarily varying along the oral-aboral axis of the body column (Fig. 1), we chose to make an axial cut across the body column to remove select cell types from the animal. Our rationale was that these resections would remove entire or nearly entire groups of neuronal cell types. We then allowed ~ 6 - 12 hours for the animal to recover. This recovery time helps to reduce the confounding contributions from initial tissue regeneration and allows animals to recover enough to tolerate microfluidic immobilization. This period is long enough to allow the wounds to close, the molecular response to injury to be completed[62,63] and the initial molecular events of regeneration to start, but it is not long enough for the animal to regenerate the lost neurons, which takes approximately 30 - 72 hours[37,61,64,65] (Supp. Fig. 5). To limit the stress from microfluidic immobilization that could exacerbate the resection wounds and affect activity, we shortened the duration of these experiments for the majority of the animals (40 min total, 20 min of no stimulation, 20 min of stimulation - valve on 1 sec at 22 psi or 0 psi, off 30 sec; first 40 min of stimulus protocol shown in Fig. 2c). Only three animals per each condition (stimulated and non-stimulated, and 5 different resections) were experimented on with a longer duration protocol as used previously (100 min total, 20 min no stimulation, 60 min of stimulation - valve on 1 sec at 22 psi or 0 psi, off 30 sec, 20 min no stimulation; stimulus protocol shown in Fig. 2c).

We began resection studies by creating “footless” *Hydra* by removing the peduncle and basal disk because we hypothesized that aboral neurons may be important for coordinating and enhancing body contractions (Fig. 3). This hypothesis was based on the fact that the activity of aboral neurons has a strong correlation with body contractions. In addition, the neuropeptide Hym-176C has been shown to induce ectodermal muscle contractions and is selectively expressed in the ectodermal peduncle neurons[66–69]. Finally, the presence of gap junction protein innexin-2 in aboral neurons could facilitate fast electrical conductions that allows these neurons to fire synchronously[47,55]. This could be necessary for enhancing neuromuscular signaling for body contractions. Because our previous measures of contraction responses were based on calcium spikes in the peduncle neurons, we used the line expressing GCaMP7b in the ectodermal epitheliomuscular cells to measure contractions pulses and bursts by averaging calcium activity in all the epitheliomuscular cells (Fig. 3a,b).

Surprisingly, our experiments with “footless” animals showed that the aboral nerve ring is not required to regulate spontaneous contractions or mechanosensory responses. After we removed the peduncle network in *Hydra*, we found the magnitude of increase in contractile activity with stimuli (or mechanosensory response) in “footless” individuals was similar to the increase in activity observed in whole individuals (“Footless” N = 8 animals stimulated 20 min, Cohen’s d = 1.89, Cliff’s delta = 0.81, $p < 0.01$); Whole N = 8 animals stimulated 20 min, Cohen’s d = 1.80, Cliff’s delta = 1.00, $p < 0.01$; Fig 3b,c). Furthermore, we found no significant difference in either the spontaneous contraction probability or the mechanosensory response probability of “footless” animals and whole animals which was a surprising result (“Footless” N = 3 animals not stimulated, spontaneous contraction probability = 0.13 ± 0.01, mean ± SEM; “Footless” N = 3 animals stimulated for 60 min, mechanosensory response probability = 0.88 ± 0.05, mean ± SEM) (Whole N = 3 animals not stimulated, spontaneous contraction probability = 0.15 ± 0.01, mean ± SEM; Whole N = 3 animals stimulated for 60 min, mechanosensory response probability = 0.73 ± 0.07, mean ± SEM; Fig. 4a,b, Supp. Movie 4-7). Because neurons in the foot fire synchronously with body contractions, we had expected changes in contraction behaviors to be significantly affected by their removal[56,57,70], but this was not what we observed.

Oral region plays a major role in mechanosensory response in *Hydra*

While the mechanosensory response in *Hydra* remained unaffected with the removal of the aboral nerve ring, we found that removal of the hypostome and tentacles (or “headless” *Hydra*) resulted in significant changes in both the mechanosensory response and spontaneous contractions. When we measured the mechanosensory response in “headless” *Hydra,* we found that the animals still responded to mechanical stimulation with a significant increase in their

contractile activity, however, they did so with a lower magnitude compared to whole and "footless" individuals ("Headless" N = 8 animals stimulated for 20 min, $p<0.01$, Cohen's d = 1.37, Cliff's delta = 1.00; Fig. 3b,c). Specifically, the "headless" *Hydra* responded with (~2.5x) lower probability compared to whole animals, and they also showed a (~3.3x) lower probability of spontaneous contraction ("Headless" N = 3 animals stimulated for 60 min, mechanosensory response probability = 0.29 ± 0.02, mean ± SEM; "Headless" N = 3 animals not stimulated, spontaneous response probability = 0.05 ± 0.01, mean ± SEM; Fig. 4a,b, Supp. Movie 8 and 9).

To verify the reduction in mechanical response probability was specific to removing the oral network of neurons, and not simply the result of injury, we performed experiments with animals that we cut longitudinally along the body axis ("bisected" *Hydra*) to remove approximately the same amount of tissue while preserving neuron in both the oral and aboral networks. We found that these longitudinally "bisected" animals showed mechanosensory responses that was not significantly different from that of the whole, "headless" or "footless" animals ("Bisected" N = 3 animals stimulated for 60 min, mechanosensory response probability = 0.54 ± 0.14, mean ± SEM; Fig. 4b). However, the magnitude of increase in contractile activity due to stimulation in "bisected" individuals, though lower than whole and "footless" individuals, was larger than "headless" individuals ("Bisected" N = 8 animals stimulated for 20 min, $p < 0.001$, Cohen's d = 2.32, Cliff's delta = 1.0). This suggests that our observations in "headless" *Hydra* were indeed dependent upon the types of neurons that were removed during the headless resection and not simply an injury response. We also found that these longitudinally "bisected" animals had a lower probability of spontaneous contraction than the whole animals but higher than "headless" animals, suggesting the entire network needs to be intact for normal contractions and the loss of roughly half the network leads to some reduction in contractile activity ("Bisected" N = 3 animals not stimulated, spontaneous contraction probability = 0.08 ± 0.02, mean ± SEM; Fig. 4a; Supp. Movie 10 and 11).

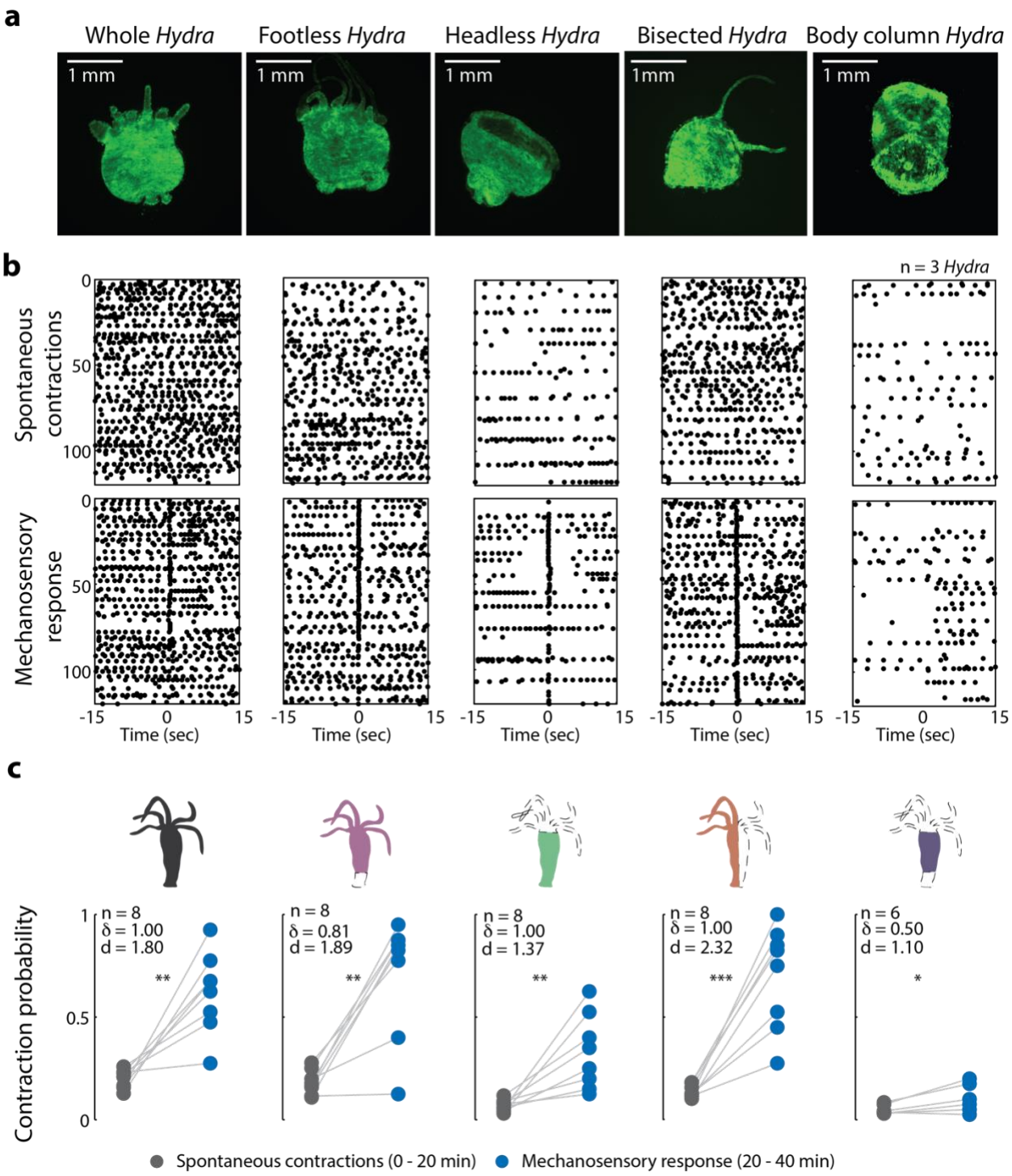

Figure 3: Oral region is important for mechanosensory response a) Representative images of resection preparations of transgenic *Hydra* during contraction (GCaMP7b, ectodermal epitheliomuscular cells): whole (or control), footless, headless, bisected and body column animal. b) Representative raster plot of stimulus time aligned spiking activity from three animals with multiple trials superimposed. Each black dot is a peak in calcium fluorescence identified as a contraction pulse. c) Gray dots are mean contraction probability during no stimulation (t=0-20 min) calculated from 1 sec window shifted by ~0.3 sec over 30 sec intervals. Blue dots are contraction probability during stimulation (t=20-40 min) calculated from 1 sec response window during valve 'on'. Light gray lines connect the probabilities for spontaneous contraction and mechanosensory response for each individual. Cartoon schematics of *Hydra* indicate the resections performed. Excised body regions outlined with a dashed line and unfilled area. Color filled body regions indicate the portion of *Hydra* experimented on. (paired t-test, n.s. = not significant; * = $p < 0.05$; ** = $p < 0.01$; *** = $p < 0.001$)

Spontaneous contractions and mechanosensory responses likely involve the same neural circuit

We next asked if the body column alone is sufficient to mediate the mechanosensory response. To answer this question, we completely removed both oral and aboral regions. In “body column” animals, we found significant reduction in both the mechanosensory response and spontaneous contractions relative to whole animals. The “body column” animals had a mechanosensory response probability that was not different from the mechanosensory response in “headless” animals, while spontaneous contraction probability was lower compared to that of “headless” animals (“Body column” N = 3 animals stimulated for 60 min, mechanosensory response probability = 0.19 ± 0.08; “Body column” N = 3 animals not stimulated, spontaneous contraction probability = 0.02 ± 0.01 mean ±SEM; Fig. 4a,b). While we found a significant increase in contractile activity with stimulation as compared to spontaneous contractile activity in “body column” individuals similar to all resections, the magnitude of the increase was the lowest in “body column” animals (even lower than “headless” animals) (”Body column” N = 6 animals stimulated for 20 min, $p < 0.05$, Cohen’s d = 1.10, Cliff’s delta = 0.50; Fig. 3b,c, Supp. Movie 12 and 13). Moreover, we did not observe significant increases in contractile activity over the same time period (comparing activity from 0 - 20 min with activity from 20 - 40 min, see ‘Methods’) in non-stimulated animals suggesting the higher probability of contractile activity was in fact due to mechanical stimulation (Supp. Fig. 6). Thus, based on the comparison between the probability of spontaneous contraction and mechanosensory response in all resections, we found that while the “body column” animals have a slightly increased contractions probability with mechanical stimulation, their ability to respond to touch is weak.

When we plotted how the different resection experiments affected the spontaneous contraction rates of the animal, we were surprised to find that changes in spontaneous contraction rates mirrored the changes in mechanosensory responses (Fig. 4a,b). In fact, when we plot the spontaneous contraction probability against the mechanosensory response probability, we find a linear relationship, which suggests that these activities share similar neural pathways (Fig. 4c). Imaging calcium activity in the neurons in whole, “bisected”, and “headless“ animals also confirms this correlation between the probability of spontaneous contraction and mechanosensory response (Supp. Fig. 7, Supp. Movie 14-17). One explanation for these results is that spontaneous contractions and mechanosensory response converge onto a single motor circuit that is responsible for body contractions, which involves the network of neurons in the hypostome and the peduncle.

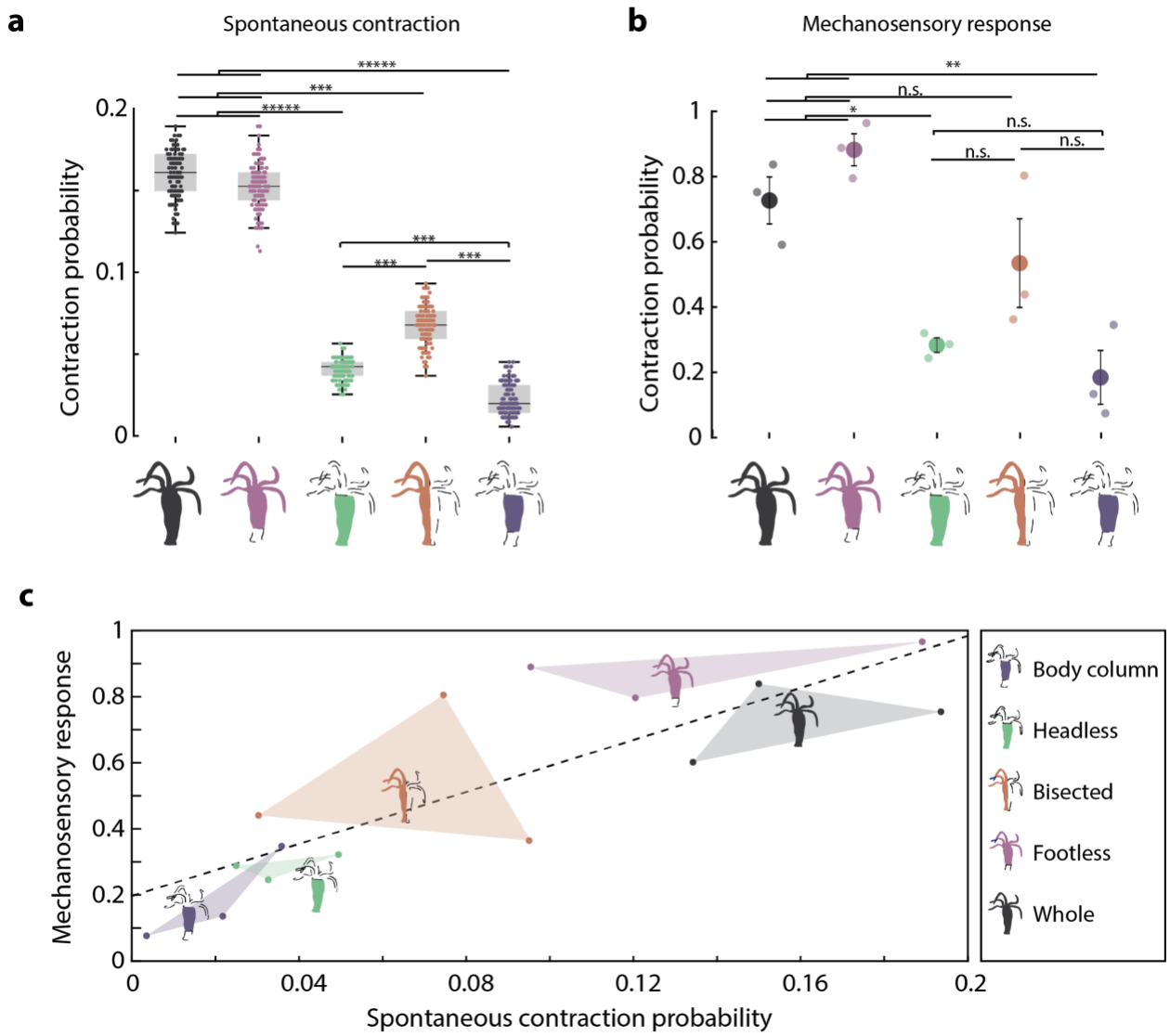

Figure 4: Surgical resections produce similar behavioral deficits in both spontaneous contractions and mechanosensory responses. a) Spontaneous contraction probability: at least one spiking event in calcium fluorescence occurring during a random 1 sec window. (1 sec window slide by ~0.3 sec across 30 sec stimulation interval; Kruskal-wallis test with post hoc dunn-sidak correction) b) Mechanosensory response probability: at least one spiking event in calcium fluorescence during the response window - 1 sec of valve on. Large opaque circles indicate average probability from all animals for each condition. Small circles indicate probability from individual animals (one-way anova with post hoc bonferroni correction). Error bars are standard error of mean (S.E.M.) (N = 3 *Hydra* for each condition; analysis from 60 min of stimulation which is t=20 min to 80 min; n.s. = not significant; * = $p < 0.05$; ** = $p < 0.01$; *** = $p < 0.001$; **** = $p < 0.0001$; ***** = $p < 0.00001$). c) Mechanosensory response probability plotted against average spontaneous contraction probability for each animal. Dashed line indicates linear regression fit. Filled circles indicate contraction probabilities from individual animals (N=3 *Hydra* for each resection). Shaded area connects the animals for each resection to indicate expected probabilities for the clusters. Cartoon schematic of *Hydra* indicates the body resections and colors from the circles (probability) match the color of resected *Hydra*.

Discussion

Our experiments with “footless”, “headless”, “bisected”, and “body column” animals show that mechanosensory and spontaneous behaviors are regulated by neural ensembles that are localized to select regions of the animal, however, some properties of the mechanosensory response may be evenly distributed throughout the body. We demonstrate that localized touch produces an increased calcium activity in both peduncle neurons (Fig. 2) and ectodermal epitheliomuscular cells (Fig. 3), which is associated with body contractions. *Hydra’s* responsiveness (i.e. probability of response to a mechanical stimuli) depends on the stimulus intensity (Fig. 2). Interestingly, we found that the “headless” and “footless” animals can still respond to mechanical stimuli despite missing the entirety of a regional nerve ring; however, “headless” animals show reduced responsiveness (Fig. 4). The “body column” animals missing both regional nerve rings have the most dramatically reduced responsiveness, suggesting that these two nerve rings work together and play compensatory roles in mediating the mechanosensory response.

Surprisingly, while the activity of peduncle neurons is strongly associated with spontaneous contractions, these neurons are not necessary for body contraction and response to mechanical stimulation. This raises the question of what role the peduncle nerve ring plays in *Hydra* behavior. One possible explanation is that this nerve ring serves to coordinate body contractions by enhancing the neural signal to ectodermal cells. Additional ~ 4 sec reduction in body contraction duration in “body column” animals compared to headless animals supports the idea that the peduncle nerve ring is also involved in coordination of contractile behavior (Supp. Fig. 8). Furthermore, calcium activity propagates from the foot to the hypostome in whole animals during body contractions[71], supporting a hypothesis that the peduncle network of neurons may be motor neurons.

Based on these observations, we propose a simple model for sensorimotor information flow in *Hydra* where we consider the hypostome as an integration point where sensory and motor information converge. The information is then communicated to the peduncle where it is amplified for coordinated whole body control. There may be sufficient functional redundancy between the hypostome and peduncle regions such that removal or damage to one of them is well tolerated in *Hydra*. Moreover, the diffuse network in the body column may retain minimal processing capabilities needed for weak sensorimotor responses.

Overall, the quantitative characterization of *Hydra’s* sensorimotor responses reported here help to build the foundation for a more comprehensive investigation of information processing in

Hydra - an animal with clear advantages to supplement commonly studied model organisms in neuroscience. Important next steps include developing mechanistic models to describe sensory information processing that supports our results. Though our experiments describe general information flow in *Hydra*, having a cellular level control of neuronal activity would be a clear advantage for revealing the function of neuronal cell types as well as their functional connectivity in the sensorimotor circuits. We expect additional future work with optogenetic manipulation of specific neuronal subtypes combined with fast, volumetric imaging techniques will provide a more comprehensive approach for characterizing this sensorimotor processing in *Hydra*. Building upon the work reported here, one can then interrogate the roles of these regional networks with multiple sensory modalities, such as light and heat, to answer questions about how diffuse nervous systems may be capable of centralized information processing and multisensory integration. These studies may help reveal a comprehensive model for how internal states and external stimuli shape the behavioral repertoire in an organism with a highly dynamic neural architecture.

Materials and Methods

***Hydra* strains and maintenance**

Hydra were raised in *Hydra* medium at 18°C in a light-cycled (12 hr: 12 hr; light: dark) incubator and fed with an excess of freshly hatched *Artemia* nauplii (Brine Shrimp Direct, Ogden UT, #BSEP8Z) three times a week (protocol adapted from Steele lab). All experiments were performed at room temperature with animals starved for 2 days.

The transgenic line nGreen was kindly provided by Rob Steele and was generated by microinjecting embryos with a plasmid containing the *Hydra* actin promoter driving GFP expression[67]. The transgenic strains expressing GCaMP6s under the actin promoter in neurons and in ectodermal epitheliomuscles (addgene # #102558) were developed by microinjections of the embryos by Christophe Dupre in Yuste lab (Columbia University)[56]. The transgenic strain expressing GCaMP7b in ectodermal epitheliomuscular cells was co-developed by Juliano Lab (UC Davis) and Robinson Lab (Rice University). Briefly, the plasmid with codon optimized GCaMP7b under the EF1a promoter was constructed by GenScript (www.GenScript.com). Injections were performed as previously described[72] with the following modifications: 1) injection solution was prepared by mixing 1 uL 0.5% phenol red (Sigma P0290-100ML) with 6 uL plasmid DNA solution prior to centrifugation and 2) embryos were fertilized for 1-2 hours prior to

injection. Plasmid promoters were cloned in expression vector pHyVec2 (Addgene plasmid: # 34790) using restriction sites NsiI. Plasmids were prepared by Maxiprep (Qiagen, Valencia, CA) and eluted in RNase-free water. A plasmid DNA solution of 1.4 ug/uL was injected into embryos using an Eppendorf FemtoJet 4x and Eppendorf InjectMan NI 2 microinjector (Eppendorf; Hamburg, Germany) under a Leica M165 C scope (Leica Microscopes, Inc; Buffalo Grove, Il). Viable hatchlings with mosaic expression were propagated by asexual reproduction and asexual buds were screened and selected for increasing amounts of transgenic tissue until a line was established with uniform expression in the ectodermal epithelial cells.

Hydra resections

Hydra were placed in a petri dish and covered with enough *Hydra* medium to prevent desiccation. When *Hydra* were relaxed and stationary, resections were performed with a single incision with a scalpel across the body. We referenced the published images of in-situ hybridizations of different cell types and spatial expression patterns to guide the location of incisions. For “footless” *Hydra,* an axial cut above the peduncle was made to remove ~ third of the lower body which included the peduncle and the basal disk. For “headless” *Hydra,* an axial cut below the hypostome was made to remove ~ third of the upper body which included the tentacles and the hypostome. For “bisected” *Hydra*, a transverse cut starting from the tip of the hypostome to the basal disk was made along the midline of the body. For “body column” *Hydra*, an axial cut above the peduncle was made to remove the lower body followed by another axial cut below the hypostome to remove the upper body region. This preparation resulted in an open tube body. *Hydra* were stored in an 18°C incubator after the excisions and until beginning the experiments. *Hydra* can seal open wounds within ~3-4 hours and repopulate the neuronal population to regain functionality in 30 - 72 hours (Supp. Fig 5). To allow *Hydra* time to recover but not regain the functionality of lost neuronal cell types, we performed experiments between 6 - 12 hours post amputation.

Microfluidic device fabrication

The mechanical stimulation devices are double-layer microfluidic devices with push down valves custom-designed with CAD software (L-edit) and fabricated using standard photo- and soft-lithography techniques. All master molds were fabricated with transparency photomasks and SU-8 2075 (MicroChem). The master mold for the bottom *Hydra* layer (circular chambers, 3 mm diameter) was fabricated with the height of ~ 105 - 110 um thick pattern (photoresist spun at 300rpm for 20sec, 2100 rpm for 30 sec). The master mold for the top valve layer (9 individual circular valves, 3 x 3 arrangement, 400 um diameter each) was fabricated with height of ~ 110

um thick (photoresist spun at 300rpm for 20sec, 2100 rpm for 30 sec). Polydimethylsiloxane (PDMS) Sylgard 184 was used to cast microfluidic devices from the master molds. The bottom *Hydra* layer (10:1 PDMS spun at 300rpm for 40 sec ~3 hr post mixing; cured for 12 min at 60°C) was bonded to the valve layer (~ 4 mm thick, 10:1 PDMS; cured for ~ 40 min at 60°C with holes punched for inlet ports) with oxygen plasma treatment (Harrick Plasma, 330 mTorr for 30 sec) and baked for at least 10 min at 60°C. *Hydra* Insertion ports were hole punched through the two layers for *Hydra* layer with 1.5 mm biopsy punches and the devices were permanently bonded (O2 plasma treatment, 330 mTorr for 30 sec) to 500 um thick fused silica wafer (University Wafers) and baked for at least 1 hr at 60°C. The design files for the photomasks and step-by-step fabrication protocols will be available on www.openHydra.org (under Resource hub/Microfluidics).

Hydra were immobilized and removed from the microfluidic device using syringes to apply alternating positive and negative pressures as previously reported[57]. The microfluidic devices were reused after cleaning similarly to the protocol previously reported. Briefly, the devices were flushed with deionized water, sonicated (at least 10 min), boiled in deionized water (160°C for 1 hr) and oven dried overnight.

After repeated use, the PDMS stiffness can change and affect the valve deflection and the actual force experienced by *Hydra* through the PDMS membrane. Additionally, uncontrollable conditions during the device fabrication process can also lead to small differences between devices. As a result, all data for Fig. 2 was taken with a single device and the response curve was used to calibrate (identify pressure that yielded ~ 60% response probability equivalent to 20-22 psi stimulus intensity) new devices.

Microfluidic mechanical stimulation

We used compressed air to inflate the microfluidic valves. For temporal control over valve (on/off) dynamics, we used USB-based controller for 24 solenoid pneumatic valves (Rafael Gómez-Sjöberg, Microfluidics Lab, Lawrence Berkeley National Laboratory, Berkeley, CA 94720) and custom-built Matlab GUI (available at www.openHydra.org) that allowed setting the stimulation parameters such as the duration of valve ‘on’ (1 sec), duration of valve ‘off’ (30 sec) and the duration of stimulation (60 min, 119 cycles of valve ‘on’ and ‘off’), and pre, post-stimulation acclimation/control period (20 min). We used a pressure regulator to manually control the air pressure into the valve manifold. In summary, we set the stimulation pressure with a pressure gauge to regulate the flow of air into the valve manifold. This valve manifold was

controlled with a USB valve controller that allowed us to programmatically inflate the valve (turn it ‘on’) with pressurized air with custom stimulation parameters.

To test sensory motor response to mechanical stimuli, we used pressurized air to inflate the push-down valve and cause it to press down on the *Hydra* immobilized in the bottom layer. Each experimental condition had at least three *Hydra* each. For a given condition, replication experiments were conducted on different days. After an animal was immobilized inside the *Hydra* chamber, we identified one valve (from the nine valves over the entire chamber) that was directly above the mid-body column region and that valve was selected for delivering stimuli. Although *Hydra* were free to move, we did not observe large displacement most of the time and as a result, the same valve remained in contact with the animal throughout the stimulation period.

We adjusted the air pressure using a pressure regulator for each experiment and the valves were inflated using a USB valve controller (see above). The full length stimulation experiment consisted of 20 min of no stimulation (control/acclimation), followed by 60 min of stimulation period (except habituation experiment where the stimulation period was 120 min), where valves were pulsed with constant pressure (0 (control), 5, 10, 15, 20, 22 or 25 psi) for 1 sec every 31 sec, then another 20 min of no stimulation (control/acclimation). Shorter stimulation experiment (used for whole-animal muscle imaging of various resections) consisted of 20 min of no stimulation (acclimation/control) followed by 20 min of stimulation period (valves pulsed for 1 sec every 31 sec with a constant pressure of 0 or 22psi). We chose a 20 min initial control period based on the high sensitivity to abrupt changes in light intensities (especially to blue wavelengths used for excitation of GCaMP) in *Hydra* which leads to increased contractile activity for 2 - 5 min. Even with the stimulus repeated for two hours at a constant inter-stimulus interval, we found no obvious evidence of sensitization, habituation or stimulus entrainment in *Hydra* (Supp. Fig. 9). As a result, we chose not to randomize the inter-stimulus interval.

Whole-animal imaging of neural activity at different stimulus intensities

We characterized the neural response to repeated local mechanical stimuli at 0 (control), 5, 10, 15, 20 and 25 psi pressure with animals that expressed GCaMP6s in neurons (Fig. 2). Each pressure condition was experimented with three animals on different days using the same device and stimulation protocol (valve pulsed for 1 sec every 31 sec for 60 min) to generate the pressure-response curves (total of 18 animals). Calcium fluorescence imaging for all experiments was conducted for the 1 hr and 40 min duration of the stimulation protocol (see Mechanical Stimulation subsection) on Nikon TI Eclipse inverted microscope with 20%

excitation light from Sola engine and GFP filter cube. We captured 100,000 frames at ~16Hz (50 msec exposures) with Andor Zyla 4.2 sCMOS camera with 4x4 binning using MicroManager. For imaging neural activity, 12-bit low noise camera dynamic range was used. To synchronize the stimulation onset times with imaging, we use used a data acquisition device (LabJack U3) to record the TTL frame out signal (fire-any, pin #2) from the Zyla and the valve on/off timestamps from the valve controller.

We used 4x (0.2 N.A) objective for wide-field imaging to fit the entire *Hydra* in the field of view to reduce the likelihood of *Hydra* migrating out of the imaging frame. There are neurons in the oral region (hypostome) that are co-active with aboral region (peduncle) neurons during body contractions; however, neurons in the hypostome appeared to be much sparser than those in peduncle (Supp. Movie 18). Discerning these hypostomal network neurons required higher magnification which significantly reduced the field of view such that considerable amount of nervous tissue could move in and out of the imaging plane (z-plane) or frame (xy-plane) making it difficult to obtain reliable calcium fluorescence time-series.

Whole-animal imaging of neural activity in resected animals

For experiments that involved body lesions (Supp. Fig. 6), the same experiment protocol and imaging settings as previously described (see ”whole animal imaging of neural activity at different stimulus intensities”, 20 min no stimulation, stimulation 1 sec every 31 sec for 60 min, 20 min no stimulation) were used with either 0 psi (control) or 20-22 psi (~ 60% response probability). Each condition group had three animals (total of 18 animals). The “headless” and “bisected” animals were prepared with the appropriate body regions removed as described previously (*“Hydra* resections”). Due to difficulty in tracking neurons and weak GCaMP expression in body column neurons, we were unable to quantify response from “footless” and “body column” *Hydra* and thus excluded from experiments.

Whole-animal imaging of epitheliomuscular activity in resected animals

We characterized the muscle response to mechanical stimuli using animals that expressed GCaMP7b under the EF1a promoter in ectodermal epitheliomuscular cells (Fig. 3). We measured contraction pulses and contraction bursts by averaging calcium activity in all the epitheliomuscular cells (Fig. 3a). The correlation between peduncle nerve ring activity and muscle contractions has been previously established based on simultaneous electrophysiology and neuronal[57] or ectodermal epitheliomuscular cells calcium imaging (Supp. Fig. 2). The imaging protocol for epitheliomuscular cells was similar to the imaging of neural activity (see

“whole animal imaging of neural activity at different stimulus intensities”), except a 16-bit camera dynamic range was used to avoid saturating the sensor.

We first developed a partial psychometric curve for calcium activity of epitheliomuscular cells to confirm the dependence of response on stimulus intensity. Three animals were imaged for 20 min without stimulation then stimulated at three different pressures (20 min at 15psi, 20 min at 20 psi, 20 min at 25psi; or in reverse order) and the epitheliomuscular response curve was used to identify the stimulus intensity (~ 22psi) which yielded ~ 60% response probability (Supp. Fig. 3). This stimulation intensity was selected for stimulation of animals with different body regions removed.

The various body regions were removed as described previously (*“Hydra* resections”) to prepare “headless”, “footless”, “bisected” and “body column” *Hydra*. Note, this transgenic line of *Hydra* expressing GCaMP7b in the ectodermal cells showed some signs of deficit. They were particularly sensitive to being handled and were more likely to dissociate after ~30 min in the chambers during long-term microfluidic immobilization and fluorescence imaging. The resected *Hydra* were especially difficult to image for the entire 1 hr 40 min without any cell dissociation. This could be due to the different promoter used for driving GCaMP expression or that phototoxicity is higher when there is a high expression of GCaMP in a larger number of cells. Because the lesioned animals were more likely to be damaged during microfluidic immobilization, the mechanical stimulation protocol (see Mechanical Stimulation subsection) was shortened to total of 40 min of imaging with 20 min of no stimulation followed by 20 min of repeated stimulation (1 sec every 31 sec for 20 min). For three animals per each resection (total of 30 animals), we used the full length protocol (1 hr 40 min of imaging; 20 min of no stimulation, 60 min of stimulation every 31 sec, 20 min of no stimulation) to obtain higher statistical power for quantifying response probability (Fig. 4). Total of 6-8 animals were stimulated for each resection condition (whole, N = 6 not-stimulated, N=8 stimulated; “footless”, N = 4, not-stimulated, N=8 stimulated; “headless”, N = 5 not-stimulated, N=8 stimulated; “bisected”, N = 5 not-stimulated, N=8 stimulated; “body column” N = 3 stimulated, N = 6 stimulated; total 61 animals, Fig. 3; 30 of which were experimented with long (1 hr 40 min) stimulation protocol Fig. 4).

Analysis of calcium activity

To analyze neural response, we used the average fluorescence from the peduncle region. Tracking individual neural responses was difficult due to high deformability of the body and lack

of fluorescence marker when neurons were not active, as a result we looked at the synchronous firing activity of the neurons in the peduncle region which is known to have high correlation with body contractions. To analyze epitheliomuscular response, we used average fluorescence from the whole animal to obtain the fluorescence signal over time and analyzed these signals similarly to neural response. Briefly, using imageJ we used a ROI over the peduncle region or the whole *Hydra* to obtain fluorescence signal over time for neuronal or epitheliomuscular calcium activity, respectively.

From the fluorescence signal, we detected the large calcium spikes as individual contractions (contraction pulses or bursts) using Matlab peak finding algorithm. We generated a raster plot of calcium spiking activity time-aligned with the stimulus where each row represented one stimulation trial with 15 sec before and after stimulation onset. These raster plots were used to calculate the probability for spontaneous contraction and mechanosensory response.
For contractile behavior analysis, we then annotated the calcium spikes. Single calcium spikes were labeled as single pulse contraction. A volley of calcium spikes was labeled as a contraction burst. Both of these led to behavioral contractions, thus time between contractions was calculated as the time between the end of a contraction event (single pulse or burst) and the start of the next one (as shown in Supp. Fig. 8). Percent of contractions that are single pulse contractions was calculated as the fraction behavioral contractions that were single calcium spikes (not bursts). Contraction duration was used to indicate the amount of time contraction behavior lasted (time from rise in fluorescence signal to return to baseline, as shown in Supp. Fig. 8)

Analyzing mechanosensory response

To obtain the response probability, which is whether or not an animal had a contraction (either a single pulse or a pulse from a burst) at the time of stimulation (when valve was pressurized), we generated a raster plot of fluorescence peaks time-aligned to stimulus onset and superimposed for each 30 sec interval (time between stimulus). We used an hour of activity (t = 20-80 min) to generate the raster plot and calculate response probability. We defined the 1 sec window while the valve was pressed as the response window for each trial (Supp. Fig. 1). Then calculated the fraction of all trials (119 trials over 60 min or 40 trials over 20 min) per animal that had at least one fluorescence spike in the 1 sec response window following stimulus onset to obtain the contraction probability. Extraction of raw fluorescence for ROIs was performed with ImageJ and post-processing analysis was performed with Matlab. One-way ANOVA with bonferroni correction was used for statistical analysis.

For animals with shorter experiment duration, the mechanosensory response probability in stimulated animals was calculated over the 20 min segment (time = 20-40 min) with a fraction of all trials (40 trials over 20 min) that had at least one fluorescence spike. Paired t-test was used to compare the difference between probability of spontaneous contraction and mechanosensory probability in the same animals for each of the conditions. The effect size (the magnitude of difference) was measured with Cohen's d and Cliff's delta.

Analyzing spontaneous contraction

For non-stimulated animals, fluorescence activity from one hour of activity (time = 20 - 80 min) was converted into a raster plot with multiple (119 trials over 60 min) 30 sec long intervals (to match the stimulation interval in stimulated animals). We obtained 'stimulation times' using a DAQ to record the signal from valve controller except the air pressure was set to 0 psi. The spontaneous contraction probability was calculated by taking the average of response probability from a random 1 sec interval (Fig. 3 and 4c). Briefly, by sliding a 1 sec window by ~0.3 sec over the x axis (30 sec of stimulation interval) on the raster plot, we generated the distribution of the fraction of trials (119 trials over 60 min) with at least one contraction event in a random 1 sec response window (Fig. 4a). The distributions were compared with Kruskal-wallis test for statistical analysis.

For animals with shorter experiment duration, spontaneous contraction probability in stimulated animals was calculated similar to non-stimulated animals above, except the raster plot was generated with the first 20 min of fluorescence activity (time = 0 to 20 min) when no stimulation was applied. Briefly, we generated a distribution of random probabilities by sliding a 1 sec window over the x-axis on the raster plot and used the mean of the distribution as the spontaneous contraction probability to compare with mechanosensory response probability from the same animal with paired t-test (Fig. 3). For non-stimulated animals with shorter experiment duration, spontaneous contraction probability was also calculated over the second 20 min interval (t = 20-40 min) to confirm the increase in contraction probability during mechanical stimulation was in fact due to stimuli and not just from temporal variation in spontaneous contractions (Supp. Fig. 6). Note, these experiments were performed with *Hydra* constrained to ~110um thick microfluidic chambers. Although animals are able to behave under such confinements, the range of behavioral motifs and rates may be altered due to compression.

References

1. Clark, D. A., Freifeld, L. & Clandinin, T. R. Mapping and Cracking Sensorimotor Circuits in Genetic Model Organisms. *Neuron* (2013). doi:10.1016/j.neuron.2013.05.006
2. Ghosh, D. D., Nitabach, M. N., Zhang, Y. & Harris, G. Multisensory integration in C. elegans. *Current Opinion in Neurobiology* (2017). doi:10.1016/j.conb.2017.01.005
3. Kaplan, H. S., Nichols, A. L. A. & Zimmer, M. Sensorimotor integration in Caenorhabditis elegans: A reappraisal towards dynamic and distributed computations. *Philos. Trans. R. Soc. B Biol. Sci.* (2018). doi:10.1098/rstb.2017.0371
4. Ahrens, M. B. *et al.* Brain-wide neuronal dynamics during motor adaptation in zebrafish. *Nature* (2012). doi:10.1038/nature11057
5. Chen, X. *et al.* Brain-wide Organization of Neuronal Activity and Convergent Sensorimotor Transformations in Larval Zebrafish. *Neuron* (2018). doi:10.1016/j.neuron.2018.09.042
6. Haesemeyer, M., Robson, D. N., Li, J. M., Schier, A. F. & Engert, F. A Brain-wide Circuit Model of Heat-Evoked Swimming Behavior in Larval Zebrafish. *Neuron* (2018). doi:10.1016/j.neuron.2018.04.013
7. Hill, A. J., Mansfield, R., Lopez, J. M. N. G., Raizen, D. M. & Buskirk, C. Van. Cellular Stress Induces a Protective Sleep-like State in C. elegans. *Curr. Biol.* 1–7 (2014). doi:10.1016/j.cub.2014.08.040
8. Raizen, D. M. *et al.* Lethargus is a Caenorhabditis elegans sleep-like state. *Nature* **451**, 569–72 (2008).
9. Artiushin, G. & Sehgal, A. The Drosophila circuitry of sleep–wake regulation. *Curr. Opin. Neurobiol.* **44**, 243–250 (2017).
10. Guo, F., Holla, M., Díaz, M. M. & Rosbash, M. A Circadian Output Circuit Controls Sleep-Wake Arousal in Drosophila. *Neuron* **100**, 624-635.e4 (2018).
11. Kayser, M. S. & Biron, D. Sleep and development in genetically tractable model organisms. *Genetics* (2016). doi:10.1534/genetics.116.189589
12. Gandhi, A. V., Mosser, E. A., Oikonomou, G. & Prober, D. A. Melatonin Is required for the circadian regulation of sleep. *Neuron* (2015). doi:10.1016/j.neuron.2015.02.016
13. Zhdanova, I. V., Wang, S. Y., Leclair, O. U. & Danilova, N. P. Melatonin promotes sleep-like state in zebrafish. *Brain Res.* (2001). doi:10.1016/S0006-8993(01)02444-1
14. Zimmerman, J. E., Naidoo, N., Raizen, D. M. & Pack, A. I. Conservation of sleep: insights from non-mammalian model systems. *Trends in Neurosciences* (2008). doi:10.1016/j.tins.2008.05.001
15. Kanaya, H. J. *et al.* A sleep-like state in *Hydra* unravels conserved sleep mechanisms during the evolutionary development of the central nervous system. *Sci. Adv.* **6**,

eabb9415 (2020).

16. Broussard, G. J., Liang, R. & Tian, L. Monitoring activity in neural circuits with genetically encoded indicators. *Front. Mol. Neurosci.* **7**, 97 (2014).

17. Chen, T.-W. *et al.* Ultrasensitive fluorescent proteins for imaging neuronal activity. *Nature* **499**, 295–300 (2013).

18. Lemon, W. C. *et al.* Whole-central nervous system functional imaging in larval Drosophila. *Nat. Commun.* **6**, 7924 (2015).

19. Prevedel, R. *et al.* Simultaneous whole- animal 3D imaging of neuronal activity using light-field microscopy. *Nat. Methods* **11**, 727–730 (2014).

20. Ahrens, M. B., Orger, M. B., Robson, D. N., Li, J. M. & Keller, P. J. Whole-brain functional imaging at cellular resolution using light-sheet microscopy. *Nat Methods* **10**, 413–420 (2013).

21. Cong, L. *et al.* Rapid whole brain imaging of neural activity in freely behaving larval zebrafish (Danio rerio). *Elife* **6**, e28158 (2017).

22. Kim, D. H. *et al.* Pan-neuronal calcium imaging with cellular resolution in freely swimming zebrafish. *Nat. Methods* **14**, 1107–1114 (2017).

23. Portugues, R., Feierstein, C. E., Engert, F. & Orger, M. B. Whole-brain activity maps reveal stereotyped, distributed networks for visuomotor behavior. *Neuron* **81**, 1328–1343 (2014).

24. Vladimirov, N. *et al.* Light-sheet functional imaging in fictively behaving zebrafish. *Nat. Methods* **11**, 883 (2014).

25. Gonzales, D. L., Badhiwala, K. N., Avants, B. W. & Robinson, J. T. Bioelectronics for Millimeter-Sized Model Organisms. *iScience* **23**, 100917 (2020).

26. Nguyen, J. P. *et al.* Whole-brain calcium imaging with cellular resolution in freely behaving Caenorhabditis elegans. *Proc. Natl. Acad. Sci.* **113**, E1074–E1081 (2016).

27. Nichols, A. L. A., Eichler, T., Latham, R. & Zimmer, M. A global brain state underlies C. elegans sleep behavior. *Science (80-.).* **356**, eaam6851 (2017).

28. Gonzales, D. L., Zhou, J., Fan, B. & Robinson, J. T. A microfluidic-induced C. elegans sleep state. *Nat. Commun.* **10**, 1–13 (2019).

29. Aimon, S. *et al. Fast near-whole-brain imaging in adult drosophila during responses to stimuli and behavior*. *PLoS Biology* **17**, (2019).

30. Dupre, C. & Yuste, R. Non-overlapping Neural Networks in *Hydra* vulgaris. *Curr. Biol.* **27**, 1085–1097 (2017).

31. Badhiwala, K. N., Gonzales, D. L., Vercosa, D. G., Avants, B. W. & Robinson, J. T. Microfluidics for electrophysiology, imaging, and behavioral analysis of: *Hydra*. *Lab Chip* **18**, 2523–2539 (2018).

32. Bargmann, C. I. & Horvitz, H. R. Chemosensory neurons with overlapping functions direct

chemotaxis to multiple chemicals in C. elegans. *Neuron* **7**, 729–742 (1991).

33. Bargmann, C. I. & Avery, L. Laser Killing of Cells in Caenorhabditis elegans. *Methods Cell Biol.* **48**, 225–250 (1995).

34. El Bejjani, R. & Hammarlund, M. Neural regeneration in Caenorhabditis elegans. *Annu. Rev. Genet.* **46**, 499–513 (2012).

35. Kroehne, V., Freudenreich, D., Hans, S., Kaslin, J. & Brand, M. Regeneration of the adult zebrafish brain from neurogenic radial glia-type progenitors. *Development* **138**, 4831–4841 (2011).

36. Hecker, A., Schulze, W., Oster, J., Richter, D. O. & Schuster, S. Removing a single neuron in a vertebrate brain forever abolishes an essential behavior. *Proc. Natl. Acad. Sci. U. S. A.* **117**, 3254–3260 (2020).

37. Itayama, T. & Sawada, Y. Development of electrical activity in regenerating aggregates of *Hydra* cells. *J. Exp. Zool.* **273**, 519–26 (1995).

38. Soriano, J., Rüdiger, S., Pullarkat, P. & Ott, A. Mechanogenetic coupling of *Hydra* symmetry breaking and driven turing instability model. *Biophys. J.* **96**, 1649–1660 (2009).

39. Gierer, A. *et al.* Regeneration of *Hydra* from Reaggregated Cells. *Nat. New Biol.* **239**, 98–101 (1972).

40. Burnett, A. L. & Diehl, N. A. The nervous system of *Hydra*. I. Types, distribution and origin of nerve elements. *J. Exp. Zool.* **157**, 217–226 (1964).

41. Lfntz, T. L. & Barrnett, R. J. Fine structure of the nervous system. *Am. Zool.* (1965).

42. Bode, H. R., Heimfeld, S., Koizumi, O., Llttlefield, C. L. & Yaross, M. S. Maintenance and regeneration of the nerve net in *Hydra*. *Integr. Comp. Biol.* **28**, 1053–1063 (1988).

43. Campbell, R. D. Tissue dynamics of steady state growth in *Hydra* littoralis. III. Behavior of specific cell types during tissue movements. *J. Exp. Zool.* **164**, 379–391 (1967).

44. Bode, H. *et al.* Quantitative analysis of cell types during growth and morphogenesis in *Hydra*. *Wilhelm Roux Arch. f*[illegible]*r Entwicklungsmechanik der Org.* **171**, 269–285 (1973).

45. Epp, L. & Tardent, P. The distribution of nerve cells in*Hydra* attenuata Pall. *Wilhelm Roux's Arch. Dev. Biol.* **185**, 185–193 (1978).

46. Koizumi, O. *et al.* Nerve ring of the hypostome in *Hydra*. I. Its structure, development, and maintenance. *J. Comp. Neurol.* **326**, 7–21 (1992).

47. Siebert, S. *et al.* Stem cell differentiation trajectories in *Hydra* resolved at single-cell resolution. *Science (80-.).* **365**, eaav9314 (2019).

48. Trembley, A., Pronk, C., Schley, J. van der & Lyonet, P. *Mémoires pour servir à l'histoire d'un genre de polypes d'eau douce, à bras en forme de cornes* . **c.1**, (Chez Jean & Herman Verbeek, 1744).

49. Mast, S. O. REACTIONS TO TEMPERATURE CHANGES IN SPIRILLUM, *HYDRA*, AND FRESH-WATER PLANARIANS. *Am. J. Physiol. Content* **10**, 165–190 (1903).

50. Wagner, G. Memoirs: On Some Movements and Reactions of *Hydra*. *J. Cell Sci.* **s2-48**, 585–622 (1905).
51. Rushforth, N. B. Inhibition of contraction responses of *Hydra*. *Integr. Comp. Biol.* **5**, 505–513 (1965).
52. Rushforth, N. B. ., Burnett, A. L. . & Maynard, R. Behavior in *Hydra* : Contraction Responses of *Hydra* pirardi to Mechanical and Light Stimuli. *Am. Assoc. Adv. Sci.* **139**, 760–761 (1963).
53. Rushforth, N. B. & Burke, D. S. Behavioral and electrophysiological studies of *Hydra*. II. Pacemaker activity of isolated tentacles. **140**, 502–519 (1971).
54. CAMPBELL, R. D., JOSEPHSON, R. K., SCHWAB, W. E. & RUSHFORTH, N. B. Excitability of nerve-free *Hydra*. *Nature* **262**, 388–390 (1976).
55. Takaku, Y. *et al.* Innexin gap junctions in nerve cells coordinate spontaneous contractile behavior in *Hydra* polyps. *Sci. Rep.* **4**, 1–8 (2014).
56. Dupre, C. & Yuste, R. Non-overlapping Neural Networks in *Hydra* vulgaris. *Curr. Biol.* **27**, 1085–1097 (2017).
57. Badhiwala, K. N., Gonzales, D. L., Vercosa, D. G., Avants, B. W. & Robinson, J. T. Microfluidics for electrophysiology, imaging, and behavioral analysis of *Hydra*. *Lab Chip* **18**, 2523–2539 (2018).
58. Vaidya, A. R., Pujara, M. S., Petrides, M., Murray, E. A. & Fellows, L. K. Lesion Studies in Contemporary Neuroscience. *Trends Cogn. Sci.* **23**, 653–671 (2019).
59. Krug, K., Daniel Salzman, C. & Waddell, S. Understanding the brain by controlling neural activity. *Philos. Trans. R. Soc. B Biol. Sci.* **370**, 1–4 (2015).
60. PASSANO, L. M. & McCULLOUGH, C. B. Co-ordinating systems and behaviour in *Hydra*. I. Pacemaker system of the periodic contractions. *J. Exp. Biol. 41 643-664, 1964* 643–664 (1964).
61. Pierobon, P. Regional modulation of the response to glutathione in *Hydra* vulgaris. *J. Exp. Biol.* **218**, 2226–2232 (2015).
62. Cazet, J. & Juliano, C. Oral Regeneration Is the Default Pathway Triggered by Injury in *Hydra*. *bioRxiv* 2020.07.06.189811 (2020). doi:10.1101/2020.07.06.189811
63. Tursch, A., Bartsch, N. & Holstein, T. W. MAPK signaling links the injury response to Wnt-regulated patterning in *Hydra* regeneration. *bioRxiv* 2020.07.06.189795 (2020). doi:10.1101/2020.07.06.189795
64. Bode, H. R. Head regeneration in *Hydra*. *Dev. Dyn.* **226**, 225–236 (2003).
65. Goel, T., Wang, R., Martin, S., Lanphear, E. & Collins, E.-M. S. Linalool acts as a fast and reversible anesthetic in *Hydra*. *PLoS One* **14**, e0224221 (2019).
66. Yum, S. *et al.* A Novel Neuropeptide, Hym-176, Induces Contraction of the Ectodermal Muscle in *Hydra*. *Biochem. Biophys. Res. Commun.* **248**, 584–590 (1998).

67. Siebert, S. *et al.* Stem cell differentiation trajectories in *Hydra* resolved at single-cell resolution. *bioRxiv* 460154 (2018). doi:10.1101/460154
68. Noro, Y. *et al.* Regionalized nervous system in *Hydra* and the mechanism of its development. *Gene Expr. Patterns* (2019). doi:10.1016/J.GEP.2019.01.003
69. Klimovich, A. *et al.* Prototypical pacemaker neurons interact with the resident microbiota. *Proc. Natl. Acad. Sci. U. S. A.* **117**, 17854–17863 (2020).
70. Shimizu, H. & Fujisawa, T. Peduncle of *Hydra* and the heart of higher organisms share a common ancestral origin. *Genesis* **36**, 182–186 (2003).
71. Szymanski, J. R. & Yuste, R. Mapping the Whole-Body Muscle Activity of *Hydra* vulgaris. *Curr. Biol.* **29**, 1807-1817.e3 (2019).
72. Juliano, C. E., Lin, H. & Steele, R. E. Generation of Transgenic *Hydra* by Embryo Microinjection. *J. Vis. Exp.* (2014). doi:10.3791/51888

Acknowledgements

We thank Dr. Rob Steele (UC Irvine), Dr. Christophe Dupre (Harvard University), and Dr. Rafael Yuste (Columbia University) for sharing transgenic *Hydra*. We also thank Dr. Guillaume Duret and Dr. Caleb Kemere for useful discussions. The promoter sequence for EF1a for generating transgenic *Hydra* was provided by Jack Cazet (UC Davis, Juliano lab) and the plasmid with GCAMP7b was cloned (and codon optimized) by GenScript. The open source USB valve controller was built based on the design by Rafael Gómez-Sjöberg, Microfluidics Lab, Lawrence Berkeley National Laboratory, Berkeley, CA 94720. This work is funded by NSF EDGE. K.N.B. is funded by a training fellowship from the Keck Center of the Gulf Coast Consortia on the NSF IGERT: Neuroengineering from Cells to Systems 1250104. We also thank the Rice Shared Equipment Authority and nanofabrication cleanroom facility where the devices were fabricated.

Author Contributions

K.N.B. conceived, performed, and analyzed experiments. J.T.R. directed the research. A.S.P. and C.E.J. generated transgenic *Hydra*. K.N.B. and J.T.R. co-wrote the paper. All authors read and commented on the manuscript.

Competing interests

The authors declare no competing interests.